


Electrokinetic-Noise-Assisted Barrier Crossing in a Nanofluidic Environment

Shayan Lameh¹, Tim Zhao¹, and Derek Stein^{1*}

Department of Physics, Brown University, Providence, Rhode Island 02912, USA

 (Received 8 May 2021; revised 21 July 2021; accepted 22 July 2021; published 11 August 2021)

We experimentally and theoretically study the dynamics of DNA driven by artificial electrokinetic noise back and forth between neighboring nanopits inside a nanofluidic device. The dynamics are consistent with a noise-assisted barrier-crossing process, exhibiting a rapid increase in the hopping rate with noise level beyond a threshold. A simple Arrhenius model with a fixed energy barrier of several $k_B T$ describes the hopping dynamics well at low noise levels but to accurately describe the dynamics over a wider range, we develop a numerical model that additionally accounts for the lateral extent of the free-energy landscape. The experimental and numerical methods reported here significantly expand the range of noise levels and time scales over which activated DNA hopping processes can be controlled and investigated.

DOI: [10.1103/PhysRevApplied.16.024019](https://doi.org/10.1103/PhysRevApplied.16.024019)

I. INTRODUCTION

Nearly 100 years have passed since Kramers started work on reaction rates [1] that led to a general theory of barrier-crossing processes [2]. Kramers's theory now serves as a model for phenomena ranging from chemical reactions [3], to major shifts of Earth's climate [4–6], to crashes in the stock market [7,8]. The theory relates the noise in a system (i.e., its intrinsic fluctuations) to the rate K at which the system overcomes an energetic barrier. Barrier-crossing phenomena in fluidic environments, including molecular sieving [9–11], giant acceleration of diffusion [12–14], and escape of trapped molecules from confinement [15–18], are normally driven by fundamental thermal fluctuations. Such phenomena are interesting and potentially technologically useful but the boiling point of the liquid severely limits the range over which the thermal noise can be varied experimentally. Kramers's theory, which applies equally well to nonthermal noise sources, illuminates ways around that limitation.

We recently reported a method for injecting a controllable level of electrokinetic noise into a fluidic device and thereby amplify the Brownian motion of DNA polymers [19]. Here, we use electrokinetic noise to control the rate of DNA hopping over an entropic barrier in a nanofluidic device. We use electrokinetic noise to explore noise levels and hopping rates that would require thermal temperatures exceeding 2000 K to achieve. We also present a numerical model of the DNA dynamics that accounts for the shape and extent of the free-energy landscape and that sheds light on time scales that are either too short or too long to be measured experimentally.

Nanofluidic devices confine ultrasmall volumes of fluid and molecules in geometries that can be arbitrarily defined by nanofabrication. The nanofluidics field began with pioneering work by the groups of Austin and then Craighead [15,20,21], who sought to create artificial gels for separating DNA molecules by length. The confining environment of nanofluidic systems enables us to probe statistical [22–24] and dynamical properties [25–28] of single molecules. Many unique DNA transport phenomena, including size-dependent DNA mobility in pressure-driven fluid flows [29], field-dependent electrophoretic mobility [30], giant acceleration of diffusion [14], and entropophoresis [31], also arise from interactions between a polymer coil and its confining environment. By defining topographic features within a nanofluidic device, it is in fact possible to sculpt the entropic landscape experienced by confined molecules nearly arbitrarily [11,32–35]. This ability makes nanofluidics well suited to create the free-energy landscape illustrated in Fig. 1 to study noise-assisted barrier crossing.

Figure 1(b) illustrates a device with two neighboring nanopits that creates a free-energy landscape for DNA with two entropic traps. The free energy of DNA is relatively low inside a nanopit because it can explore more configurations and increase its configurational entropy there. The height of the free-energy barrier between the nanopits is determined by the confining dimensions, in particular the height of the constriction separating the nanopits [34,36].

II. METHODS

A nanofluidic device is fabricated on a glass chip with a nanoslit of height $a = 75$ nm, length $L = 3.5$ mm, and width $160 \mu\text{m}$ [Fig. 1(b)]. Two U-shaped microchannels, each $0.5 \mu\text{m}$ deep, connect the nanoslit to two pairs

*derek_stein@brown.edu

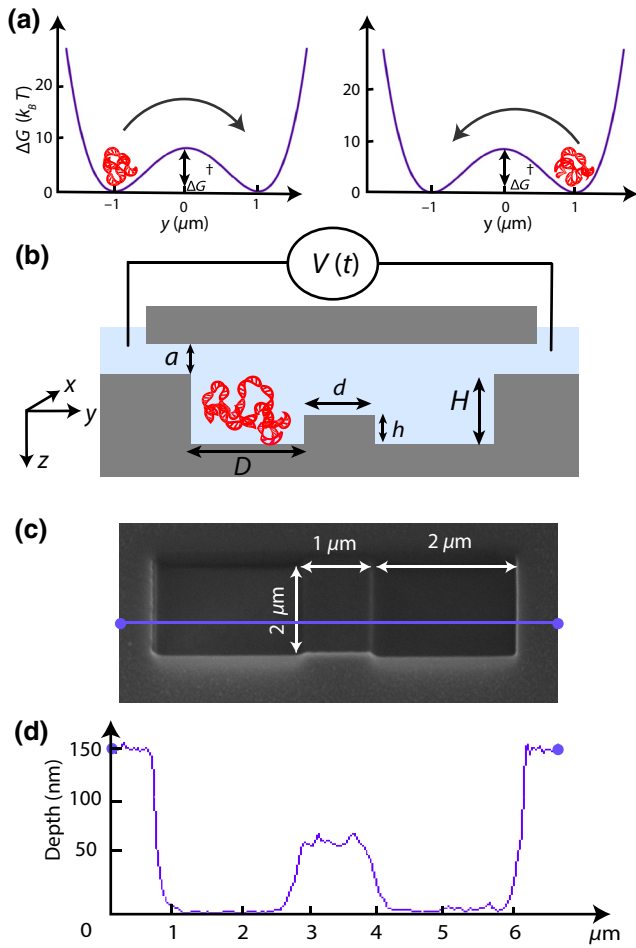


FIG. 1. Noise-assisted hopping. (a) A schematic of DNA hopping between two free-energy minima separated by a barrier of height ΔG^\ddagger . (b) A nanofluidic device cross section with two nanopits that create entropic traps for a DNA molecule. The sketch shows the voltage noise source and the dimensions H , h , D , d , and a . (c) A scanning electron micrograph of nanopits viewed from above. (d) A height profile measured across a pair of nanopits, as indicated by the blue line in (c).

of reservoirs. We use standard techniques described previously [14,33,34] to pattern and etch the nanoslit and microchannels into the device. To create a pair of pits, a focused-ion-beam (FIB) machine first mills a $2 \times 5 \mu\text{m}$ trench within the slit and then mills deeper in two square regions at both ends of the rectangle. Figure 1(c) shows a scanning-electron-microscope (SEM) image of a typical double pit. The square pits with width $D = 2 \mu\text{m}$ are separated by an obstacle with width $d = 1 \mu\text{m}$. Figure 1(d) shows the profile of the double pit scanned by an atomic force microscope. The pits are $H = 150 \text{ nm}$ deep and the obstacle between them rises a height $h = 50 \text{ nm}$ above that. The purpose of the raised obstacle is to create an entropic barrier in the free-energy landscape for confined DNA that molecules need to overcome in order to move

to the neighboring pit. A surface roughness with a peak-to-peak range of approximately 10 nm , as measured by atomic force microscopy, is the main source of experimental uncertainty in theoretical estimates of the free-energy barrier; we parametrize the uncertainty in h and H with the 3.5 nm rms roughness.

λ DNA (48.5 kbp, New England Biolabs) is fluorescently stained with YOYO-I dye at a 10: 1 base-pair-to-dye ratio. The DNA is suspended in 20 mM Tris-EDTA buffer that is titrated to pH 8.0 using HCl and 4% v/v β -mercaptoethanol is added to suppress photobleaching. The suspension is diluted to a final DNA concentration of $0.2 \mu\text{g/mL}$ before being introduced into the nanofluidic device.

We image the DNA using an optical microscope (Nikon TE2000-U) with a $60\times$ water-immersion objective lens with a numerical aperture of 1.20 and a digital camera (Andor iXon). A 120-W metal-halide lamp (EXFO X-Cite 120) supplies ultraviolet light for fluorescence imaging. A physical shutter (Uniblitz Model VCM-D1) is used to limit the exposure time and thereby mitigate photobleaching of the stained DNA molecules. Videos of 100 images are recorded with a 50-ms exposure time and intervals of $\Delta t = 500 \text{ ms}$ between frames. We confirm that the optical images of the double-pit structures show no measurable distortion when compared with atomic force microscopy profiles of the same devices.

Finally, we apply a recently described technique to inject electrokinetic noise into the nanofluidic device and study its effects on the DNA dynamics [19]. Briefly, a digital-to-analog voltage controller (National Instruments) applies a time-dependent noise voltage $V(t)$ across the nanoslit. $V(t)$ has Gaussian fluctuations with an adjustable standard deviation, σ_e , zero mean, and a finite bandwidth Δf . The resulting electric field induces a fluctuating force in the y direction on confined molecules, as illustrated in Fig. 1(b). The applied voltage is related to the resulting DNA velocity by the electrophoretic mobility, $\mu = v/V(t)$, which accounts for the electrophoretic DNA motion through the fluid and the electro-osmotic flow of fluid within the channel.

Figure 2 shows representative λ -DNA trajectories under the influence of different levels of applied noise. With a low noise level of $\sigma_e = 6 \text{ V}$, a molecule remains trapped within a single pit for the 50-s duration of the measurement [Fig. 2(a)]. With $\sigma_e = 12 \text{ V}$, an identical molecule hops between the two pits about seven times in total, with apparently random intervals of time between each hop [Fig. 2(b)]. $\sigma_e = 18 \text{ V}$ results in about 20 hops in the same time interval [Fig. 2(c)]. We note that we only track molecules that are at least $20 \mu\text{m}$ away from the edges of the $160 \mu\text{m}$ slit in order to avoid possible edge effects.

The data in Fig. 2(b) show that the DNA molecule occasionally straddles two pits simultaneously for more than a single frame of the video. This indicates that DNA may

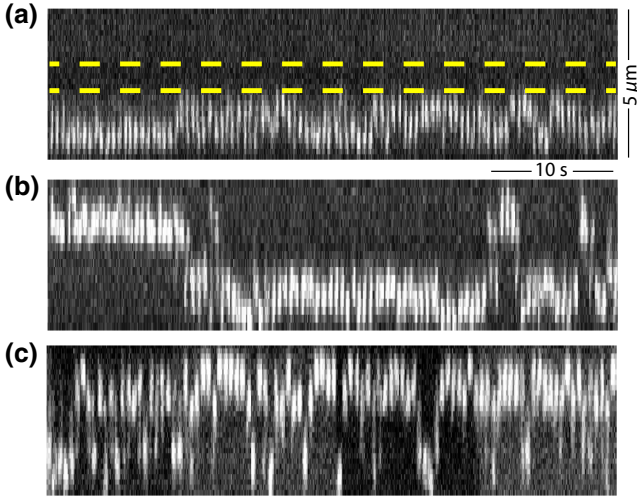


FIG. 2. A montage of time-resliced fluorescence images of a λ -DNA molecule hopping between neighboring nanopits with (a) $\sigma_e = 6$ V, (b) $\sigma_e = 12$ V, and (c) $\sigma_e = 18$ V applied across the fluidic device: the boundaries between the pits and the central obstacle are shown in (a). The outer boundaries of the pits reach the upper and lower boundaries of the image. The contrast and brightness of the images are adjusted for clarity.

require more time than the 0.5-s interval between images to overcome the central obstacle, especially for low values of σ_e . We also note that in Fig. 2(c), the molecule occasionally hops back and forth between the two pits with every frame. This suggests that the crossing time may be significantly shorter than the 0.5-s interval between frames when σ_e is large. Taken together, the observations emphasize that in our measurements the DNA cannot move the distance between pits instantaneously; nor can the camera resolve the fastest crossing rates. To build a theoretical understanding of the dynamics, we develop a numerical model that takes these important physical factors into account.

We simulate a point particle in a bistable potential with a fixed energy barrier, as illustrated in Fig. 1(a). The dynamics are described by a Langevin equation for an overdamped Brownian particle at position y ,

$$\dot{y} = -\frac{dG(y)}{dy} \frac{1}{\zeta} + \sqrt{\frac{2D_{\text{eff}}}{dt}} dW_t, \quad (1)$$

where D_{eff} is the effective diffusion coefficient under σ_e , ζ is the drag coefficient, and W_t is a standard Wiener process with $\langle dW_t^2 \rangle = dt$. As we have reported previously [19], D_{eff} is related to σ_e^2 and the thermal diffusivity, D_0 , by $D_{\text{eff}} = D_0 + \alpha\sigma_e^2$, where $\alpha = \mu^2/4\Delta fL^2$. D_0 depends on the confinement of the nanofluidic device. However, D_0 is expected to vary only modestly between the different parts of the double-pit structure. When a molecule is above the central barrier, the effective slit height is 175 nm and $D_0 \approx 0.08 \mu\text{m}^2/\text{s}$ and when the molecule is in either pit, the effective slit height is 225 nm and $D_0 \approx 0.11 \mu\text{m}^2/\text{s}$.

For the purpose of simplifying our numerical-model calculations, we implement a uniform diffusivity. The value $D_0 \approx 0.09 \mu\text{m}^2/\text{s}$ that we use corresponds to the diffusivity of λ DNA in a slit of intermediate height $H = 200$ nm, based on its bulk radius of gyration $R_g = 0.69 \mu\text{m}$, its bulk self-diffusion coefficient $D_{\text{bulk}} = 0.46 \mu\text{m}^2/\text{s}$ [37], and the previously measured relationship between D_0 , D_{bulk} , R_g , and H for DNA confined in a nanoslit [38]. It is reasonable to base estimates of DNA diffusivity in our device on theory and measurements of DNA in slits, because the in-plane radius of gyration for λ DNA confined in a 200 nm deep slit is about $0.7 \mu\text{m}$ [39]; hence a molecule at the center of a $2 \mu\text{m} \times 2 \mu\text{m}$ square pit should not significantly interact with the pit edges. The double-well potential $\Delta G(y) = -c_2 y^2 + c_4 y^4$ is sketched in Fig. 1(a). The parameters $c_2 = 12.2k_B T (\mu\text{m})^{-2}$ and $c_4 = 6.1k_B T (\mu\text{m})^{-4}$ describe a free-energy landscape with a barrier of height $\Delta G^\ddagger = 6.2 \pm 0.4k_B T$ between the two minima; we obtain that value of ΔG^\ddagger from a theoretical scaling model of the confinement free energy that has previously been validated [33,36,40,41] (for details of the calculations, see the Supplemental Material [42]). The minima of the free-energy landscape are located at $y = \pm 1 \mu\text{m}$, which is where we estimate that the λ -DNA coil begins to interact with the physical obstacle. We simulate trajectories by solving Eq. (1) using Euler's method in PYTHON with a time step of $dt = 1$ ms.

Figure 3 compares experimental and simulated DNA trajectories over 50 s intervals at different σ_e . Custom

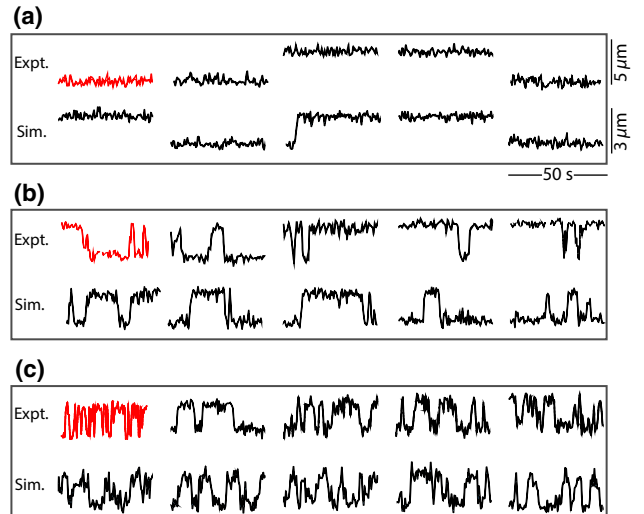


FIG. 3. Representative trajectories of DNA molecules in the y direction are presented from measurements and simulations with (a) $\sigma_e = 6$ V, (b) $\sigma_e = 12$ V, and (c) $\sigma_e = 18$ V. The vertical scale bars are $5 \mu\text{m}$ for the experimental traces and $3 \mu\text{m}$ for the simulations. The horizontal scale bars are 50 s. The red trajectories correspond to the molecules represented in Fig. 2. The simulated trajectories are sampled every $\Delta t = 500$ ms, matching the experiments.

image-analysis software [14,19,33] is used to obtain the DNA center-of-mass (c.m.) location every $\Delta t = 500$ ms from the video recordings. The simulated trajectories presented in Fig. 3 are also sampled every $\Delta t = 500$ ms, although the trajectories are computed using a time step of $dt = 1$ ms. The measured and simulated trajectories corresponding to the same noise intensity are both qualitatively and quantitatively similar, with the understanding that an exact correspondence of stochastic trajectories is not to be expected. With $\sigma_e = 6$ V, none of the five measured DNA trajectories show a hop, while only a single hop occurs within the five simulated trajectories. As σ_e increases to 12 V, the frequency of hops increases to about five per 50 s interval for both the measured and the simulated trajectories. At $\sigma_e = 18$ V, the hops occur so frequently in both the measurements and the simulations that it becomes difficult to distinguish individual hops by eye.

To systematize our analysis of noise-assisted hopping, we define a hop by the following rule: a successful hop occurs when the c.m. escapes the boundary of one pit and subsequently enters the boundary of the neighboring pit. The relevant boundaries are illustrated as yellow dashed lines in Fig. 2(a).

III. RESULTS

Figure 4 shows the relationships between the hopping rate and σ_e . In measurements, DNA molecules are stably

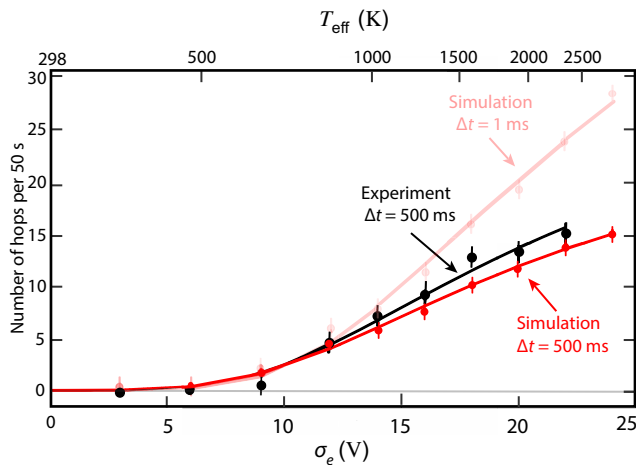


FIG. 4. The σ_e dependence of the mean number of DNA hops between nanopits in a 50 s interval. The black dots are mean experimental hops from at least 40 DNA molecules. The dark red dots represent mean hops from 100 simulated trajectories sampled at $\Delta t = 500$ ms. The light red dots are mean hops from the same simulated trajectories but sampled at $\Delta t = 1$ ms. The error bars show the standard error. The solid curves are fits of Eq. (3) to the data, obtaining $K_0 = 0.64$ s $^{-1}$ and $\Delta G^\ddagger = 7.7k_B T$ for the experiments, $K_0 = 0.54$ s $^{-1}$ and $\Delta G^\ddagger = 7.4k_B T$ for the simulations with $\Delta t = 500$ ms, and $K_0 = 1.23$ s $^{-1}$ and $\Delta G^\ddagger = 10.1k_B T$ for the simulations with $\Delta t = 1$ ms.

pinned in one pit or the other for low values of σ_e . The hopping rate increases rapidly from 0.01 s $^{-1}$ to 0.26 s $^{-1}$ as σ_e increases from 9 V to 18 V, beyond which value the hopping rate begins to saturate. The results from the simulated trajectories closely follow the measured results when the sampling rates match ($\Delta t = 500$ ms). However, when the same simulated trajectories are sampled every $\Delta t = 1$ ms, the number of hops detected increases more rapidly beyond $\sigma_e = 9$ V; the hopping rate reaches 0.47 s $^{-1}$ at $\sigma_e = 22$ V, as compared with 0.27 s $^{-1}$ with $\Delta t = 500$ ms. An explanation for this discrepancy is that some back-and-forth hops that complete in less than 500 ms are undetectable in trajectories sampled at $\Delta t = 500$ ms, whereas they can be observed with $\Delta t = 1$ ms. The discrepancy is low at low σ_e because rapid hops are less likely to occur.

The σ_e -dependent hopping rate seen in Fig. 4 is reminiscent of a thermally activated barrier-crossing process, except that in this case, electrokinetic noise plays the role of temperature. We have previously reported how the addition of electrokinetic noise across a nanoslit amplifies Brownian dynamics in a way that can be characterized by an effective temperature [19]:

$$T_{\text{eff}} = T(1 + \alpha\sigma_e^2). \quad (2)$$

Combining Eq. (2) with the Arrhenius equation, we obtain a simple model of the noise-assisted hopping rate,

$$K = K_0 \exp \left[-\frac{\Delta G^\ddagger}{k_B T(1 + \alpha\sigma_e^2)} \right], \quad (3)$$

where K_0 is the attempt rate and ΔG^\ddagger is the barrier height. We fit Eq. (3) to the data in Fig. 4, using K_0 and ΔG^\ddagger as fit parameters. The Arrhenius rate and the DNA hopping rate both rise rapidly beyond a certain effective temperature threshold. The fits follow each data set closely and the measured and simulated trajectories with $\Delta t = 500$ ms yield comparable values for K_0 and ΔG^\ddagger .

The shortcomings of the simple Arrhenius model are revealed by the fits of Eq. (3) to the data in Fig. 4. Consider the simulated trajectories: whereas the true barrier height is $\Delta G^\ddagger = 6.1k_B T$, the fit of Eq. (3) yields a somewhat higher value, $\Delta G^\ddagger = 7.4k_B T$, for $\Delta t = 500$ ms, and a significantly higher value, $\Delta G^\ddagger = 10.1k_B T$, for $\Delta t = 1$ ms. Furthermore, the fit value of K_0 is inconsistent; the value obtained with $\Delta t = 500$ ms is less than half the value obtained with $\Delta t = 1$ ms. Why does the Arrhenius model fall short? The model only considers a fixed free-energy barrier between two stable states, without accounting for the distance between them or the time it takes an object to travel that distance. That approximation is reasonable for low σ_e , where the DNA molecule is strongly confined and spends most of the time inside a pit. However, for high σ_e , the DNA molecule hops frequently across the free-energy landscape and the time it spends in transit between

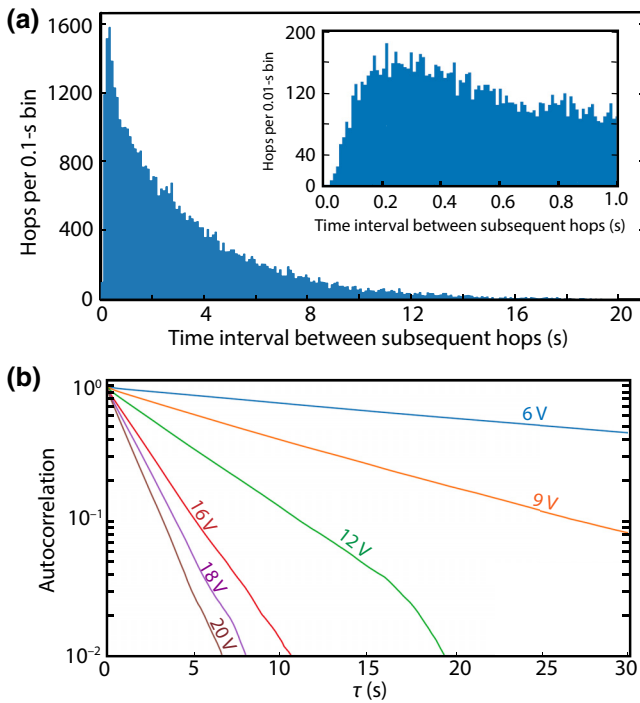


FIG. 5. The statistics of the simulated hopping trajectories. (a) The distribution of time intervals between subsequent hops for a 100 000-s simulated trajectory with $\sigma_e = 20$ V. The inset shows short-time detail of the same distribution. (b) The autocorrelation of the y position with τ for simulated trajectories with $\sigma_e = 6, 9, 12, 16, 18,$ and 20 V.

the pits becomes a significant fraction of the total time. A model must account for the finite distance between the free-energy minima to accurately describe the dynamics at high σ_e .

Figure 5(a) shows the distribution of intervals between subsequent hops of a simulated molecule. The distribution shows an exponential decay on long time intervals (> 1 s), which is a hallmark of a noise-activated barrier-crossing process. On short time intervals, there is a delay before the distribution exhibits a decaying character; the frequency of hopping intervals rises from zero to the peak value over the range 0–0.2 s. The finite time it takes a molecule to travel across the barrier explains that relative dearth of short hopping intervals.

Figure 5(b) plots the position autocorrelation, C_y , of a simulated particle as a function of the lag time, τ , for $\sigma_e = 6, 9, 12, 16, 18,$ and 20 V. C_y decays exponentially with τ and higher σ_e is associated with a faster rate of decay. From the slopes of the curves in Fig. 5(b), we find the characteristic decay times to be 35, 11, 4.6, 2.2, 1.7, and 1.4 s, ordered by increasing values of σ_e .

IV. DISCUSSION AND CONCLUSIONS

We show that it is possible to create a bistable fluidic device for a DNA molecule and controllably increase the

DNA hopping rate between the two stable sites with artificial electrokinetic noise (Fig. 1). The resulting DNA hops correspond to thermally activated barrier crossing at an effective temperature that is adjustable well above temperatures at which DNA can survive (Fig. 4). It is worth noting that the actual thermal temperature is not changed; we confirm using a thermocouple that the device temperature increases by only 0.1°C after an hour of applying the highest electrokinetic noise level, $\sigma_e = 22$ V. The curves in Fig. 4 are experimental and simulation fits of the noise-induced hopping rate between the stable states using the Arrhenius equation given in Eq. (3) with two fit parameters, attempt rate K_0 , and barrier height ΔG^\ddagger .

The Arrhenius model explains the hopping rate of confined DNA polymers under electrokinetic noise reasonably well at low noise levels but Figs. 3–5 are evidence that the Arrhenius model deviates significantly at higher noise levels. For example, Fig. 3 highlights the significant amount of time that the DNA molecules spend between the stable sites at high noise level, which is not accounted for in the Arrhenius model. Figure 4 shows that different sampling rates of the same simulated trajectories produce different parameters under the Arrhenius model. The inset of Fig. 5(a) shows the violation of the instantaneous-transition assumption under the Arrhenius model. The shortcomings of an Arrhenius model can be overcome with a numerical model of Brownian particle dynamics in an extended free-energy landscape that accounts for the distance between the two stable sites. The parameters of the free-energy landscape used in the model can be obtained from Flory scaling theory; remarkably accurate predictions are obtained with a scaling prefactor of 1. Additionally, the numerical simulations offer a way to study the DNA hopping dynamics on much shorter time scales (< 0.2 s) and longer time scales (> 60 s) than we can probe experimentally. We conclude that this numerical approach makes superior quantitative predictions of the dynamics and offers better theoretical insight into the noise-assisted hopping process for DNA.

An ability to control the hopping rate of DNA across free-energy barriers could open avenues for fundamental studies and biotechnological applications. For example, stochastic resonance (SR) is a general phenomenon that could be realized with a single DNA. SR refers to the collaboration of white noise with a weak time-varying signal in a bistable system where an optimum noise level enhances the effect of the weak signal. To experimentally study SR for a particle over an entropic barrier, one needs access to an extremely wide range of noise levels without varying the barriers height. The indicator of SR would be to see the synchronization between a weak periodic driving force and the hopping of the particle back and forth over an entropic barrier.

There is also an opportunity to study how artificial noise influences the rates at which DNA molecules cross

biologically relevant constrictions. In particular, passing DNA across barriers such as the blood-brain barrier [43–45] and endosomes [46–49] is a major obstacle in gene therapy. Electroporation is a technique of applying electric field pulses across a cell to increase the cell membrane permeability, which is a proven method of increasing the gene-transfer efficiency *in vivo* and *in vitro* [50–52]. However, the strength of the electric field and the duration of exposure that cells can survive severely limits the technique; for example, tests on brain endothelial cells have found that cell death grows increasingly likely as 50-ms electric field pulses increase beyond approximately 250 V/cm [44,45]. We speculate that electrokinetic noise, the strong electric fields of which have a mean of zero, may pose a relatively reduced risk to the cells, while the effect of increasing the barrier-crossing rate might promote gene transfection. Fundamental research along these lines could lead to improved biotechnologies and therapeutic methods.

-
- [1] J. A. Christiansen and H. A. Kramers, About the speed of chemical reactions, *Z. Phys. Chem.* **104**, 451 (1923).
- [2] H. A. Kramers, Brownian motion in a field of force and the diffusion model of chemical reactions, *Physica* **7**, 284 (1940).
- [3] P. Hänggi, P. Talkner, and M. Borkovec, Reaction-rate theory: Fifty years after Kramers, *Rev. Mod. Phys.* **62**, 251 (1990).
- [4] R. Benzi, G. Parisi, A. Sutera, and A. Vulpiani, Stochastic resonance in climatic change, *Tellus* **34**, 10 (1982).
- [5] A. Ganopolski and S. Rahmstorf, Abrupt Glacial Climate Changes Due to Stochastic Resonance, *Phys. Rev. Lett.* **88**, 038501 (2002).
- [6] R. Benzi, Stochastic resonance: From climate to biology, *Nonlinear Process. Geophys.* **17**, 431 (2010).
- [7] J.-P. Bouchaud and R. Cont, A Langevin approach to stock market fluctuations and crashes, *Eur. Phys. J. B—Condens. Matter Complex Syst.* **6**, 543 (1998).
- [8] D. Valenti, B. Spagnolo, and G. Bonanno, Hitting time distributions in financial markets, *Phys. A: Stat. Mech. Appl.* **382**, 311 (2007).
- [9] P.-G. De Gennes, Passive entry of a DNA molecule into a small pore, *Proc. Natl. Acad. Sci.* **96**, 7262 (1999).
- [10] M. Muthukumar, Translocation of a Confined Polymer through a Hole, *Phys. Rev. Lett.* **86**, 3188 (2001).
- [11] J. Fu, J. Yoo, and J. Han, Molecular Sieving in Periodic Free-Energy Landscapes Created by Patterned Nanofilter Arrays, *Phys. Rev. Lett.* **97**, 018103 (2006).
- [12] G. Costantini and F. Marchesoni, Threshold diffusion in a tilted washboard potential, *EPL (Europhys. Lett.)* **48**, 491 (1999).
- [13] P. Reimann, C. Van den Broeck, H. Linke, P. Hänggi, J. M. Rubi, and Agustín Pérez-Madrid, Giant Acceleration of Free Diffusion by Use of Tilted Periodic Potentials, *Phys. Rev. Lett.* **87**, 010602 (2001).
- [14] D. Kim, C. Bowman, J. T. Del Bonis-O'Donnell, A. Matzavinos, and D. Stein, Giant Acceleration of DNA Diffusion in an Array of Entropic Barriers, *Phys. Rev. Lett.* **118**, 048002 (2017).
- [15] J. Han and H. G. Craighead, Separation of long DNA molecules in a microfabricated entropic trap array, *Science* **288**, 1026 (2000).
- [16] A. D. Dinsmore, M. F. Hsu, M. G. Nikolaidis, M. Marquez, A. R. Bausch, and D. A. Weitz, Colloidosomes: Selectively permeable capsules composed of colloidal particles, *Science* **298**, 1006 (2002).
- [17] X. Liu, M. Mihovilovic Skanata, and D. Stein, Entropic cages for trapping DNA near a nanopore, *Nat. Commun.* **6**, 1 (2015).
- [18] N. Laachi and K. D. Dorfman, DNA electrophoresis in confined, periodic geometries: A new lakes-straits model, *J. Chem. Phys.* **133**, 12B605 (2010).
- [19] S. Lameh, L. Ding, and D. Stein, Controlled Amplification of DNA Brownian Motion Using Electrokinetic Noise, *Phys. Rev. Appl.* **14**, 054042 (2020).
- [20] W. D. Volkmuth and R. H. Austin, DNA electrophoresis in microlithographic arrays, *Nature* **358**, 600 (1992).
- [21] S. W. Turner, A. M. Perez, A. Lopez, and H. G. Craighead, Monolithic nanofluid sieving structures for DNA manipulation, *J. Vac. Sci. Technol., B: Microelectron. Nanometer Struct.—Process., Meas., Phenom.* **16**, 3835 (1998).
- [22] W. Reisner, K. J. Morton, R. Riehn, Y. M. Wang, Z. Yu, M. Rosen, J. C. Sturm, S. Y. Chou, E. Frey, and R. H. Austin, Statics and Dynamics of Single DNA Molecules Confined in Nanochannels, *Phys. Rev. Lett.* **94**, 196101 (2005).
- [23] A. Balducci, P. Mao, J. Han, and P. S. Doyle, Double-stranded DNA diffusion in slitlike nanochannels, *Macromolecules* **39**, 6273 (2006).
- [24] E. A. Strychalski, S. L. Levy, and H. G. Craighead, Diffusion of DNA in nanoslits, *Macromolecules* **41**, 7716 (2008).
- [25] O. B. Bakajin, T. A. J. Duke, C. F. Chou, S. S. Chan, R. H. Austin, and E. C. Cox, Electrohydrodynamic Stretching of DNA in Confined Environments, *Phys. Rev. Lett.* **80**, 2737 (1998).
- [26] C.-C. Hsieh, A. Balducci, and P. S. Doyle, An experimental study of DNA rotational relaxation time in nanoslits, *Macromolecules* **40**, 5196 (2007).
- [27] A. Balducci, C.-C. Hsieh, and P. S. Doyle, Relaxation of Stretched DNA in Slitlike Confinement, *Phys. Rev. Lett.* **99**, 238102 (2007).
- [28] K.-W. Hsiao, C. M. Schroeder, and C. E. Sing, Ring polymer dynamics are governed by a coupling between architecture and hydrodynamic interactions, *Macromolecules* **49**, 1961 (2016).
- [29] D. Stein, F. H. J. van der Heyden, W. J. A. Koopmans, and C. Dekker, Pressure-driven transport of confined DNA polymers in fluidic channels, *Proc. Natl. Acad. Sci.* **103**, 15853 (2006).
- [30] G. B. Salieb-Beugelaar, J. Teapal, J. van Nieuwkastele, D. Wijnperlé, J. O. Tegenfeldt, F. Lisdat, A. van den Berg, and J. C. T. Eijkel, Field-dependent DNA mobility in 20 nm high nanoslits, *Nano Lett.* **8**, 1785 (2008).
- [31] S. M. Stavis, J. Geist, M. Gaitan, L. E. Locascio, and E. A. Strychalski, DNA molecules descending a nanofluidic staircase by entropophoresis, *Lab. Chip* **12**, 1174 (2012).
- [32] W. Reisner, N. B. Larsen, H. Flyvbjerg, J. O. Tegenfeldt, and A. Kristensen, Directed self-organization of single

- DNA molecules in a nanoslit via embedded nanopit arrays, *Proc. Natl. Acad. Sci.* **106**, 79 (2009).
- [33] J. T. Del Bonis-O'Donnell, W. Reisner, and D. Stein, Pressure-driven DNA transport across an artificial nanotopography, *New J. Phys.* **11**, 075032 (2009).
- [34] E. Shelton, Z. Jiang, S. Wang, and D. Stein, Controlling the conformations and transport of DNA by free energy landscaping, *Appl. Phys. Lett.* **99**, 263112 (2011).
- [35] D. Ross, E. A. Strychalski, C. Jarzynski, and S. M. Stavis, Equilibrium free energies from non-equilibrium trajectories with relaxation fluctuation spectroscopy, *Nat. Phys.* **14**, 842 (2018).
- [36] W. Reisner, N. Larsen, H. Flyvbjerg, J. O. Tegenfeldt, and A. Kristensen, Directed self-organization of single DNA molecules in a nanoslit via embedded nanopit arrays, *PNAS* **106**, 79 (2009).
- [37] A. Balducci, P. Mao, J. Han, and P. Doyle, Double-stranded DNA diffusion in slitlike nanochannels, *Macromolecules* **39**, 6273 (2006).
- [38] D. Stein, F. H. J. van der Heyden, W. J. A. Koopmans, and C. Dekker, Pressure-driven transport of confined DNA polymers in fluidic channels, *PNAS* **103**, 15853 (2006).
- [39] J. Tang, S. L. Levy, D. W. Trahan, J. J. Jones, H. G. Craighead, and P. S. Doyle, Revisiting the conformation and dynamics of DNA in slitlike confinement, *Macromolecules* **43**, 7368 (2010).
- [40] M. Doi and S. F. Edwards, *The Theory of Polymer Dynamics* (Oxford University Press, New York, 1986).
- [41] P.-G. Gennes, *Scaling Concepts in Polymer Physics* (Cornell University Press, Ithaca, NY, 1979).
- [42] See the Supplemental Material at <http://link.aps.org/supplemental/10.1103/PhysRevApplied.16.024019> for details of the free-energy barrier calculations.
- [43] W. M. Pardridge, Blood-brain barrier delivery, *Drug. Discov. Today* **12**, 54 (2007).
- [44] M. Hjouj, D. Last, D. Guez, D. Daniels, S. Sharabi, J. Lavee, B. Rubinsky, and Y. Mardor, MRI study on reversible and irreversible electroporation induced blood brain barrier disruption, *PLoS ONE* **7**, e42817 (2012).
- [45] M. Bonakdar, E. M. Wasson, Y. W. Lee, and R. V. Davalos, Electroporation of brain endothelial cells on chip toward permeabilizing the blood-brain barrier, *Biophys. J.* **110**, 503 (2016).
- [46] L. D. Cervia, C.-C. Chang, L. Wang, and F. Yuan, Distinct effects of endosomal escape and inhibition of endosomal trafficking on gene delivery via electrotransfection, *PLoS ONE* **12**, e0171699 (2017).
- [47] S. A. Smith, L. I. Selby, A. P. R. Johnston, and G. K. Such, The endosomal escape of nanoparticles: Toward more efficient cellular delivery, *Bioconjug. Chem.* **30**, 263 (2018).
- [48] I. M. S. Degors, C. Wang, Z. U. Rehman, and I. S. Zuhorn, Carriers break barriers in drug delivery: Endocytosis and endosomal escape of gene delivery vectors, *Acc. Chem. Res.* **52**, 1750 (2019).
- [49] B. M. H. Bruininks, P. C. T. Souza, H. Ingolfsson, and S. J. Marrink, A molecular view on the escape of lipoplexed DNA from the endosome, *Elife* **9**, e52012 (2020).
- [50] T. Y. Tsong, *Electroporation of Cell Membranes*, Electroporation and Electrofusion in Cell Biology (Springer US, Boston, MA, 1989), p. 149.
- [51] J. C. Weaver, Electroporation of cells and tissues, *IEEE Trans. Plasma Sci.* **28**, 24 (2000).
- [52] J. Gehl, Electroporation: Theory and methods, perspectives for drug delivery, gene therapy and research, *Acta Physiol. Scand.* **177**, 437 (2003).